MAGLEV 2022
25th International Conference on Magnetically Levitated Systems and Linear Drives

Modeling of the Transrapid's Electromagnets and the Application to Large Mechatronic Vehicle Models

Patrick Schmid[1], Georg Schneider[1], Arnim Kargl[1],
Florian Dignath[2], Xin Liang[3], and Peter Eberhard[1]

[1] Institute of Engineering and Computational Mechanics, University of Stuttgart, Stuttgart, Germany
[2] thyssenkrupp Transrapid GmbH, Munich, Germany
[3] CRRC Qingdao Sifang Co., Ltd., Qingdao, People's Republic of China
Corresponding author: Patrick Schmid (e-mail: patrick.schmid@itm.uni-stuttgart.de).

***Abstract*—This work gives an overview of a general approach for modeling the electromagnets of a magnetic levitation (Maglev) vehicle based on electromagnetic suspension. The method intends to map the magnets' static and dynamic behavior in a frequency range relevant for use in mechatronic simulation models and Maglev control or observer design. The methodology starts with setting up the equivalent magnetic circuit considering magnetic reluctances, fringing and leakage flux, magnetic saturation, and eddy currents. Then, the resulting equations are coupled with the magnet's electric circuits using Ampère's law and Faraday's law of induction. Further, a numerical model reduction technique is sketched, which yields a simplified version of the previously derived magnet model with nearly the same input-output structure and input-output behavior, suitable for large simulation models and control design. The approach's capabilities and strengths are shown by the agreement to measurements and by implementing the resulting models in large mechatronic vehicle models of the Transrapid.**

***Index Terms*—Electromagnet Modeling, Maglev Vehicle, Magnetic Saturation, Eddy Currents, Multibody Systems, Maglev Control.**

I. Introduction

ELECTROMAGNETS realize the contactless electromagnetic suspension (EMS) of magnetic levitation (Maglev) vehicles. One representative of such EMS-based Maglev vehicles is the high-speed vehicle Transrapid [1], which operates successfully with speeds up to 430 km/h in daily operation in Shanghai between Pudong International Airport and Longyang Road Station since 2003 [2]. Meanwhile, China's Ministry of Science and Technology (MOST) drives and promotes the development and research of Maglev vehicle technology, intending to reach a maximum speed of 600 km/h [2]. The Chinese rolling stock manufacturer CRRC Qingdao Sifang Co., Ltd. recently presented the prototype of such a new Maglev vehicle to the public. The first test runs have been successfully completed. However, an improved understanding of and insight into the electromagnets' static and dynamic behavior are necessary to drive at higher speeds than hitherto traveled. To predict ride comfort, to study different scenarios, or to improve control laws, numerical simulation models are essential and powerful tools during the development process. However, the reliable usage of numerical simulation to forecast the system's behavior requires validated simulation models which map the relevant physical effects.

Different modeling techniques exist to describe an electromagnet's static and dynamic behavior. The methods differ in terms of the level of detail, the underlying mathematical equations, the computational load, or in the assumptions and limitations. Models based on the finite element method (FEM) discretize the underlying Maxwell equations and result in a possibly nonlinear system of equations. The method is the tool of choice for the initial magnet design and analysis process [3, 4] because it provides detailed static force characteristics and flux distributions. However, FEM models are unusable for a co-simulation with large mechatronic vehicle models, because of their huge computational effort, especially for transient simulations, and the challenge of describing the time-varying air gap and moving magnet. In addition, the parameterization of such models is usually non-trivial. The equivalent magnetic circuit method (EMC) is another concept to map an electromagnet's static characteristics [5, 6]. A surrogate network maps the magnetic flux path and contains different network elements to model various physical effects. However, such models often disregard the electromagnet's dynamics and neglect the effect of magnetic saturation, which becomes relevant for higher loads occurring, e.g., in failure scenarios. For these reasons, oversimplified analytical magnet models are usually used in large mechatronic vehicle models to approximate the electromagnets' static and dynamic behavior [7-9]. In addition, such analytical models often build a questionable basis for Maglev control and observer design. Except for [10], these simple analytical models usually neglect effects resulting from magnetic saturation, or eddy currents anyway, and parameterization of the surrogate parameters is often challenging. Consequently, there is a need for a general modeling approach to derive magnet models which contain the relevant physical effects to reliably map the statics and dynamics in a frequency range appropriate for use in large mechatronic simulation models.

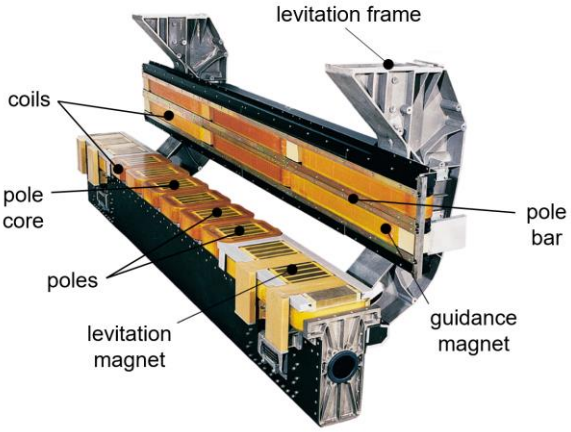

Fig. 1. Magnet module of Transrapid TR08 containing a levitation and guidance magnet. Image: thyssenkrupp Transrapid.

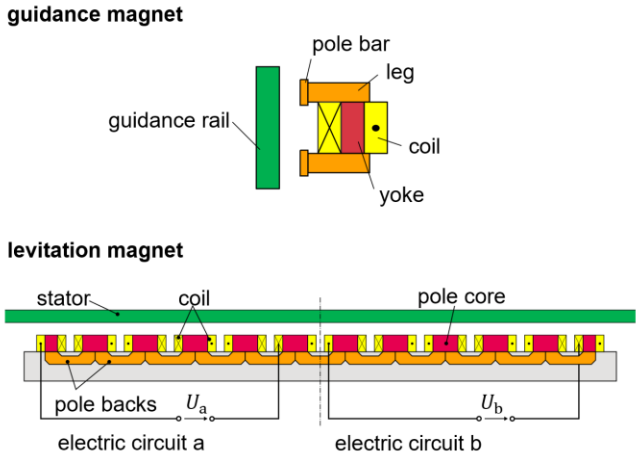

Fig. 2. Schematic cross-sectional cut of a guidance magnet and longitudinal cut of a standard levitation magnet.

Simultaneously, their usage for Maglev control and observer design or validation purpose would be beneficial. Furthermore, the computational effort of the derived models should be manageable.

The paper addresses the need for magnet models mentioned above. It gives an overview of a general approach for electromagnet modeling [11], including the effects of magnetic reluctance, fringing and leakage flux, magnetic saturation, and eddy currents. The modeling follows a systematic approach. At first, the equivalent magnetic network and its equations are set up. In the next step, the equations for the electric circuits are derived using Kirchhoff's circuit laws. By exploiting Ampère's circuital law and Faraday's law of induction, the equations of the magnetic and electric circuits are coupled. From a mathematical point of view, the entire dynamics of the electromagnet results in a high-dimensional system of differential-algebraic equations in the flux, which can be transformed into a system of differential-algebraic equations formulated in an auxiliary vector of variables of a smaller dimension. The magnetic force at each pole is derived from an energy balance and expressed in terms of the fluxes. Since this model's computational effort is significant, a simplified version is derived for control and observer design investigations or for use in mechatronic simulation models of the vehicle. For this, a numerical procedure is developed by which a more simplified current-based model is derived, which possesses the same input-output behavior as the previously derived flux-based model. Its dynamics is described by just one ordinary differential equation per underlying control loop, which depends, as well as the statics, on numerically derived characteristic diagrams. The proposed modeling approach can be applied to any levitation or guidance magnet. The model's structure allows simple integration into sizeable mechatronic simulation models.

The paper's contribution is two-part. The first part gives an overview and summary of the above-sketched electromagnet's modeling technique [11]. In contrast to the rather technical work presented in [11], it guides the reader to the main concepts and ideas without discussing technical particularities or equations in detail, respectively. The second part outlines how the previously derived magnet models can be integrated into and applied in large mechatronic vehicle models. Such models usually comprise multibody systems for the mechanics and detailed control algorithms. Further, an overview of already existing works using such derived magnet models is given.

The article is structured as follows. Section II presents the general modeling technique followed by an exemplary validation of the method through a Transrapid's levitation magnet in Sec. III. The derivation of the simplified magnet models is discussed in Sec. IV. Finally, the derived magnet models are coupled with large mechatronic simulation models in Sec. V. Section VI provides conclusions of the article.

II. Modeling

The high-speed EMS-based Transrapid-type Maglev vehicle uses an electromagnetically decoupled levitation and guidance system to account for higher loads. Figure 1 illustrates the arrangement of the separated guidance and levitation electromagnets. A schematic sketch for both magnet types is shown in Fig. 2. For a guidance magnet, the aluminum coils surround the yokes, which are connected to the pole bars by legs. For levitation magnets, aluminum coils surround the pole cores, which in turn are connected by so-called pole backs. The flux paths are closed by either the stator for the levitation magnets or the guidance rail for the guidance magnets, respectively. The poles' electrical linking differs for each magnet type, e.g., a standard levitation magnet has two electric circuits, see Fig. 2, and three electric circuits feed the poles of a levitation bow magnet installed at the front and rear of the vehicle.

Several physical effects influence the electromagnet's static and dynamic behavior, e.g., the air gap s between the magnet's pole surface and stator packs for levitation or between the magnet's pole bar and reaction rail for guidance. Moreover, the geometry and material properties of the involved iron parts cause effects like, e.g., magnetic saturation, eddy currents, or hysteresis. In addition, fringing and leakage fluxes stem from the diffusion of flux lines. As it is common practice in literature, however, it is reasonable to neglect the effect of magnetic hysteresis

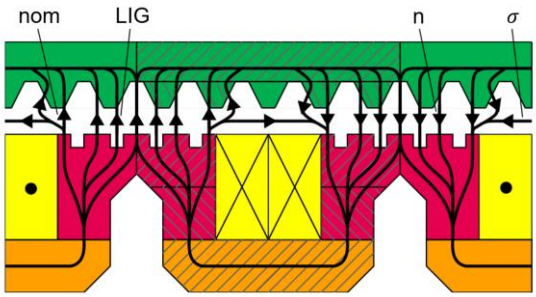

Fig. 3. Schematic path of magnetic flux for a levitation magnet consisting of nominal (nom) flux, a flux running through the linear generator notches (LIG), notch (n), and leakage (σ) flux.

and the influence of eddy currents caused by the long-stator synchronous motor. In a system-theoretical view, the electromagnets of a Maglev vehicle constitute an input-output system. The air gaps and applied voltages are the model's inputs, and the currents and magnet forces are the model's outputs.

In the first step, the general modeling approach demands setting up the electromagnet's magnetic network or equivalent magnetic circuit. For this, the path distribution of the magnetic flux is considered, which usually follows from models based on FEM. Figure 3 exemplarily illustrates an extract of the magnetic flux path for a levitation magnet. Then, the magnet's equivalent magnetic circuit (EMC) is derived based on the existing flux paths by introducing branches and nodes at appropriate locations. Figure 4 shows an exemplary extract of a levitation magnet's equivalent magnetic circuit. It contains the network's magnetic fluxes summarized by the vector $\boldsymbol{\phi} = [\phi_1, \phi_{\sigma,1}, \phi_2, \phi_{\sigma,2}, \dots]^{\mathrm{T}}$. The aluminum coils cause the magnetomotive forces, which are described by the vector $\boldsymbol{\theta} = [\theta_1, \theta_2, \dots]^{\mathrm{T}}$. The several reluctances R within the network follow the fundamental law

$$R = \frac{l}{\mu A} , \tag{1}$$

where a homogeneous material of length l with cross-section area A and permeability μ is assumed. Individual geometric conditions and material properties define the air gap reluctances R_{L}, leakage reluctances R_{σ}, and reluctances of the iron components R_{Fe} within the network. By describing the iron's permeability in terms of the flux, i.e., $\mu = \mu(\phi)$, it is possible to include the effect of magnetic saturation within the model. The equivalent magnetic circuit is equipped with so-called magnetic inductances L_{ec} to consider the effect of eddy currents. Its impact on the magnetic network is analogous to an electric inductance in an electric network. The duality of magnetic and electric networks allows applying Kirchhoff's circuit laws and Ohm's law, i.e., $\theta = R\,\phi$, for the equivalent magnetic circuits. Finally, a nonlinear system of equations results through a systematic application of the laws mentioned above.

The electromagnet's electric networks are coupled with the magnetic network in the next step, which creates the required input-output structure of the model compared to the actual system. Formally, an electromagnet's electric circuit comprises an Ohmic resistance R_{el} and an electric inductance L for each coil

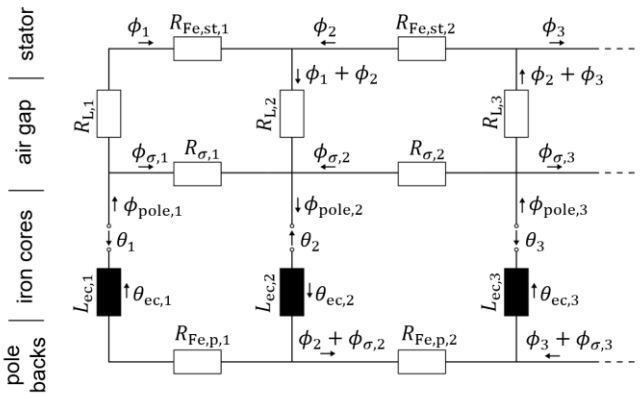

Fig. 4. Extract of a levitation magnet's equivalent magnetic circuit.

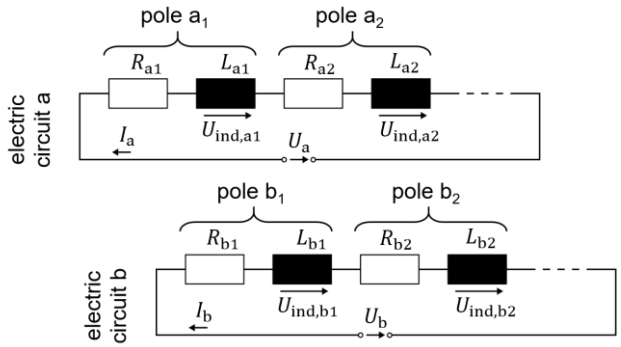

Fig. 5. Exemplary electric circuits of a levitation magnet.

surrounding a pole core. Figure 5 exemplarily illustrates both electric circuits of a levitation magnet. Ampère's law in the simplified version

$$\theta = n\,I \tag{2}$$

states the relation between the electromagnet's current I and the magnetomotive force θ in dependence on the number of coil windings n. In addition, Faraday's law of induction

$$U_{\mathrm{ind}} = n\,\dot{\phi} \tag{3}$$

describes the impact of a changing flux on the electric network characterized by the induced voltage U_{ind}. By establishing Kirchhoff's laws for the electric networks and using Ampère's law (2) and Faraday's law of induction (3) in an appropriate way, the magnetic network described by the nonlinear system of equations is coupled with the electric networks. Rewriting and reordering yields a high-dimensional differential-algebraic equation (DAE) formulated in the flux variable $\boldsymbol{\phi}$ of the form

$$\boldsymbol{M}\dot{\boldsymbol{\phi}} = -\boldsymbol{A}_{\mathrm{mag}}(\boldsymbol{s}, \boldsymbol{\phi})\,\boldsymbol{\phi} + \boldsymbol{B}\boldsymbol{U} , \tag{4}$$

which describes the electromagnet's dynamics. The matrix $\boldsymbol{A}_{\mathrm{mag}}$ contains the topology and parameters of the magnetic network. The constant matrices $\boldsymbol{M}$ and $\boldsymbol{B}$ comprise information about the structure and parameterization of the magnetic and electric networks. Note that the matrix $\boldsymbol{M}$ is singular such that Equation (4) implicitly contains algebraic equations. Now, the system's inputs, i.e., the air gaps $\boldsymbol{s}$ of each pole and the applied voltages $\boldsymbol{U}$, are the DAE's and thus the models inputs.

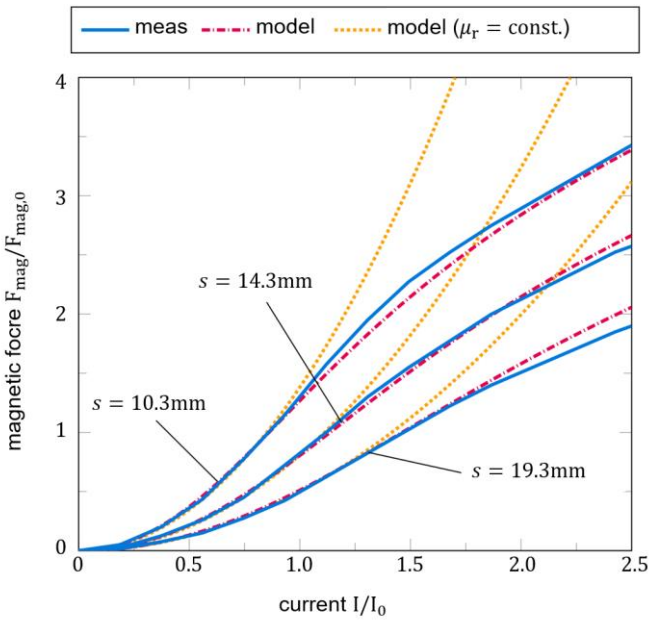

Fig. 6. Normalized force-gap-characteristics of a TR09 standard levitation magnet comparing the model obtained from the proposed modeling approach, the measurements, and a further model without considering magnetic saturation for comparison purpose.

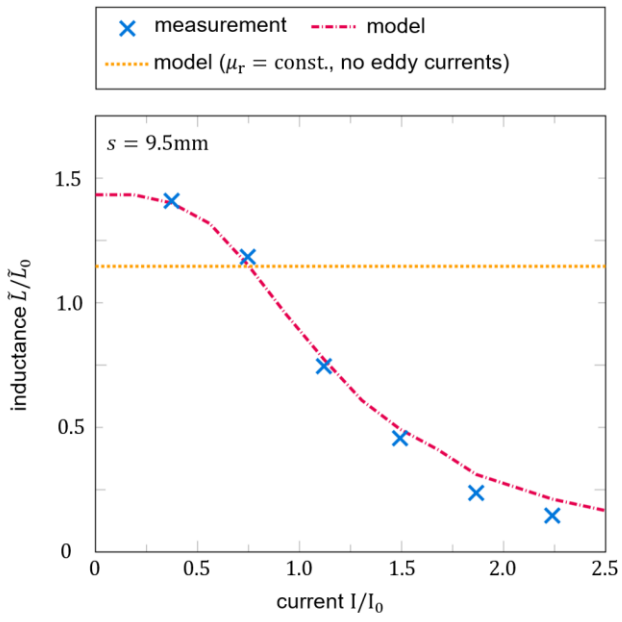

Fig. 7. Normalized inductance of a TR09 standard levitation magnet as a function of the current and air gap for the obtained model, and a model without saturation and eddy currents in comparison to measurements.

Since the DAE (4) is difficult to solve from a numerical point of view due to its structure and dimension, it is mapped in a further step onto a reduced set of coordinates. For this purpose, the substitute flux variable $\boldsymbol{\eta}$ is introduced, which describes the sum of the pole fluxes for each electric circuit. Based on further transformation steps and assumptions, the original high-dimensional DAE (4) can be expressed by a low-dimensional DAE formulated in the variables $\boldsymbol{\eta}$ and $\boldsymbol{\phi}$ in semi-explicit form

$$\begin{aligned} \dot{\boldsymbol{\eta}} &= -\widetilde{\boldsymbol{A}}_{\mathrm{mag}}(\boldsymbol{s},\boldsymbol{\phi})\boldsymbol{\eta} + \widetilde{\boldsymbol{B}}\boldsymbol{U}\,, \\ \boldsymbol{0} &= \boldsymbol{g}(\boldsymbol{s},\boldsymbol{\phi},\boldsymbol{\eta}) \end{aligned} \tag{5}$$

with adapted system matrices $\widetilde{\boldsymbol{A}}_{\mathrm{mag}}$ and $\widetilde{\boldsymbol{B}}$. Since the dependence of the flux in $\widetilde{\boldsymbol{A}}_{\mathrm{mag}}$ can not be expressed explicitly in terms of $\boldsymbol{\eta}$, the algebraic constraint $\boldsymbol{0} = \boldsymbol{g}(\boldsymbol{s},\boldsymbol{\phi},\boldsymbol{\eta})$ exists.

It remains to describe the system's outputs, i.e., the magnet force and current, based on the variables $\boldsymbol{\eta}$ and $\boldsymbol{\phi}$ of DAE (5). The magnet force F_{mag} for each pole results from considering the principle of virtual work in combination with an energy balance. It holds that

$$F_{\mathrm{mag}} = \frac{\mu_{\mathrm{r}} - 1}{2\,\mu_{\mathrm{r}}\,\mu_0\,A}\phi_{\mathrm{F}}^2\,, \tag{6}$$

where μ_{r} is the iron's permeability, μ_0 the permeability of free space, and ϕ_{F} the flux contributing to the magnet force, which can be derived from the knowledge of $\boldsymbol{\phi}$. In addition, it is possible to derive an explicit expression for the electromagnet's current $\boldsymbol{I}_L$ in the form

$$\boldsymbol{I}_L = \widetilde{\boldsymbol{C}}(\boldsymbol{s},\boldsymbol{\phi})\boldsymbol{\eta}\,, \tag{7}$$

where the output matrix $\widetilde{\boldsymbol{C}}$ depends on the air gaps $\boldsymbol{s}$ and the flux variable $\boldsymbol{\phi}$. In summary, Equations (5)-(7) represent the electromagnet's model and include the effects of magnetic reluctances, fringing and leakage flux, magnetic saturation, and eddy currents.

III. Model Analysis and Validation

A standard levitation magnet of the latest Transrapid vehicle TR09 is modeled to justify the proposed modeling technique. The parameters are chosen accordingly, compare also [11]. The underlying equations of the model are implemented and solved in MATLAB/Simulink. The simulation results are validated with measurements from a test bed of thyssenkrupp Transrapid.

The static behavior of the model is validated by employing the measured force-current-gap characteristics, see Fig. 6. The model's static behavior results from solving (5) for $\dot{\boldsymbol{\eta}} = \boldsymbol{0}$, assuming a constant air gap for all poles and choosing the voltages consonant with the currents following Ohm's law. The characteristics are also shown for a model for which the effect of magnetic saturation is neglected, as it is usually practiced in literature. The model's static behavior matches the measurements over the entire current and gap range. For $I < I_0$, one can recognize the well-known quadratic relation. As the current increases, the gradient of the magnetic force decreases for $I > I_0$ because of magnetic saturation. For this case, the simplified model without saturation clearly fails.

The inductance $\tilde{L}$ is used to validate the model's dynamics. Generally, the inductance measures how fast the electromagnet's current follows an applied voltage step. Figure 7 illustrates the measured inductance, the model's inductance, and the inductance of a model for which the effect of saturation and eddy currents is neglected. The model's inductance corresponds to the measurements for $s = 9.5\mathrm{mm}$. The model accurately maps the inductance's decrease for increasing currents mainly resulting from magnetic saturation. When neglecting saturation and eddy currents, the inductance is generally smaller and does not depend on the current. Therefore, the analysis reveals that it is essential to model the effects caused by saturation and eddy currents if the dynamic behavior is of interest.

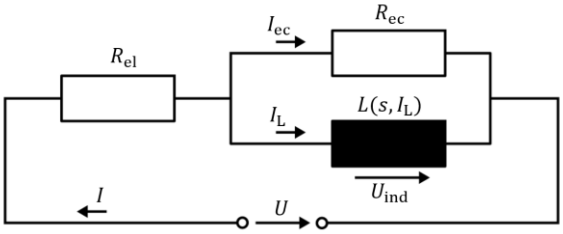

Fig. 8. Equivalent electric circuit of simplified current-based electromagnet model representing an imaginary decoupled electric circuit.

IV. Derivation of Simplified Magnet Model

The proposed modeling approach creates a flux-based model suitable for studying effects arising in the early magnet design process or for validation. Nevertheless, since its computational effort is significant, a simplified model with the same input-output structure and a comparable static and dynamic behavior is desirable. Then, such a model fits well for usage in sizeable mechatronic simulation models or for Maglev control and observer design.

A. Equations of Simplified Magnet Model

In general, the electric circuits of the electromagnets are coupled to each other via the magnetic network. For example, the flux linkage over the stator and pole back in the mid of the standard levitation magnet couples both electric circuits. The analysis in [11] reveals that the transformational coupling between the electric circuits is small and can be neglected for simplicity, i.e., if two electric circuits are supplied with their nominal voltage, a disturbance of one of them can hardly be noted in the current of the other. In addition, a substitute gap s and magnet force F_{mag} for each electric circuit is assumed. Thus, each electric circuit can be described by the equivalent electric circuit shown in Fig. 8, which results from the duality of magnetic and electric circuits. Note that in comparison to Fig. 5, the Ohmic resistance R_{el} is already summed up, and the former inductance is separated in a so-called eddy current resistance R_{ec} and electric inductance $L(s, I_{\mathrm{L}})$. Here, R_{ec} results from modeling the eddy currents by magnetic inductances in the magnetic network. Further, the joint inductance L of the simplified model is implicitly defined by the magnetic network's reluctances.

The simplified model's dynamics can be derived in terms of the current I_{L} by applying Kirchhoff's second circuit law and Faraday's law of induction again. The resulting scalar ordinary differential equation (ODE) reads as

$$\dot{I}_{\mathrm{L}} = -\frac{R_{\mathrm{el}}}{\left(\frac{R_{\mathrm{el}}}{R_{\mathrm{ec}}}+1\right)\left(\frac{\partial L(s,I_{\mathrm{L}})}{\partial I_{\mathrm{L}}} I_{\mathrm{L}} + L(s,I_{\mathrm{L}})\right)} I_{\mathrm{L}} - \frac{\frac{\partial L(s,I_{\mathrm{L}})}{\partial s}}{\frac{\partial L(s,I_{\mathrm{L}})}{\partial I_{\mathrm{L}}} I_{\mathrm{L}} + L(s,I_{\mathrm{L}})} I_{\mathrm{L}} \dot{s} + \frac{1}{\left(\frac{R_{\mathrm{el}}}{R_{\mathrm{ec}}}+1\right)\left(\frac{\partial L(s,I_{\mathrm{L}})}{\partial I_{\mathrm{L}}} I_{\mathrm{L}} + L(s,I_{\mathrm{L}})\right)} U\,, \tag{8}$$

compare [11]. The joint inductance L represents two parts, one part L_{eff} causes the magnetic force, and the other ingredient L_{σ} maps the leakage flux. The equality of the magnetic energy stored in the effective inductance L_{eff} and the work of the magnetic forces yields an expression for the magnetic force

$$F_{\mathrm{mag}} = F_{\mathrm{mag}}(s, I_L) = -\frac{\partial}{\partial s}\int_0^{I_{\mathrm{L}}} L_{\mathrm{eff}}(s, i)\; i \; di\,, \tag{9}$$

where i is the integration variable for the current, compare [7, 11].

For electromagnets with standard geometries, it is possible to describe L analytically as a function of the air gap and current or to derive L analytically by the equivalent magnetic circuit. However, this is impossible for the considered type of electromagnets whose magnetic network consists of several poles of different geometries, which are, moreover, coupled. As a result, it is necessary to derive the quantities $F_{\mathrm{mag}}(s, I_L)$, $\tilde{L}(s, I_{\mathrm{L}}) = \frac{\partial L(s,I_{\mathrm{L}})}{\partial I_{\mathrm{L}}} I_{\mathrm{L}} + L(s, I_{\mathrm{L}})$, and $\partial L(s, I_{\mathrm{L}})/\partial s$ based on the detailed flux-based model (5)-(7) in a discrete fashion in the form of characteristic diagrams using a numerical procedure.

B. Derivation of System Parameters

The Ohmic resistance R_{el} and eddy current resistance R_{ec} can be derived by the detailed flux-based model analytically, compare [11]. For parameterizing the quantities $F_{\mathrm{mag}}(s, I_L)$, $\tilde{L}(s, I_{\mathrm{L}})$, and $\partial L(s, I_{\mathrm{L}})/\partial s$, the gap and current operation ranges are discretized by an equidistant regular grid. Here, it is advantageous that both entities have lower and upper physical limits given by the Maglev vehicle's operation.

The characteristic diagram for $F_{\mathrm{mag}}(s, I_L)$ results from solving (5) and (6) for gap and current pairs spanned by the regular grid. The procedure is analogous to the study performed in Sec. III, i.e., determining the magnet's force-current-gap characteristics.

The quantities $\tilde{L}(s, I_{\mathrm{L}})$ and $\partial L(s, I_{\mathrm{L}})/\partial s$ can be derived from the detailed flux-based model by appropriately performing time integrations. For $\tilde{L}(s, I_{\mathrm{L}})$, it can be exploited that the $\tilde{L}(s, I_{\mathrm{L}})$ does not dependent on the impact of eddy currents and must hold as well for $\dot{s} = 0$. As a result, ODE (8) simplifies and can be solved analytically. Now, by performing time integrations of the detailed flux-based model under voltage steps, the time constants defining $\tilde{L}(s, I_{\mathrm{L}})$ result for each gap and current pair. In a further step, the quantity $\partial L(s, I_{\mathrm{L}})/\partial s$ can be obtained from the detailed model by applying a virtual control law $U = R_{\mathrm{el}} I_{\mathrm{L}}$. In doing so, the first and third terms of ODE (8) cancel out, and it is again possible to solve ODE (8) analytically. Then, the time constants defining $\partial L(s, I_{\mathrm{L}})/\partial s$ follow from solving the detailed flux-based model under linearly increasing gaps. Figure 9 exemplarily illustrates the obtained characteristic diagrams for the quantities $F_{\mathrm{mag}}(s, I_L)$, $\tilde{L}(s, I_{\mathrm{L}})$, and $\partial L(s, I_{\mathrm{L}})/\partial s$ for one half magnet of a standard TR09 levitation magnet.

It is worth noting that the detailed flux-based and simplified current-based models have a comparable input-output structure. Moreover, simulations reveal that the input-output behavior of the models is similar when neglecting the coupling, compare [11]. The simplified model achieves a speedup of about 277 compared to the detailed flux-based model because it is much easier to solve the underlying ODE than the DAE.

V. Application to Mechatronic Vehicle Models

The magnet models derived by the modeling approach presented in Secs. II and IV are suitable for mapping the relevant static and dynamic behavior necessary for large mechatronic

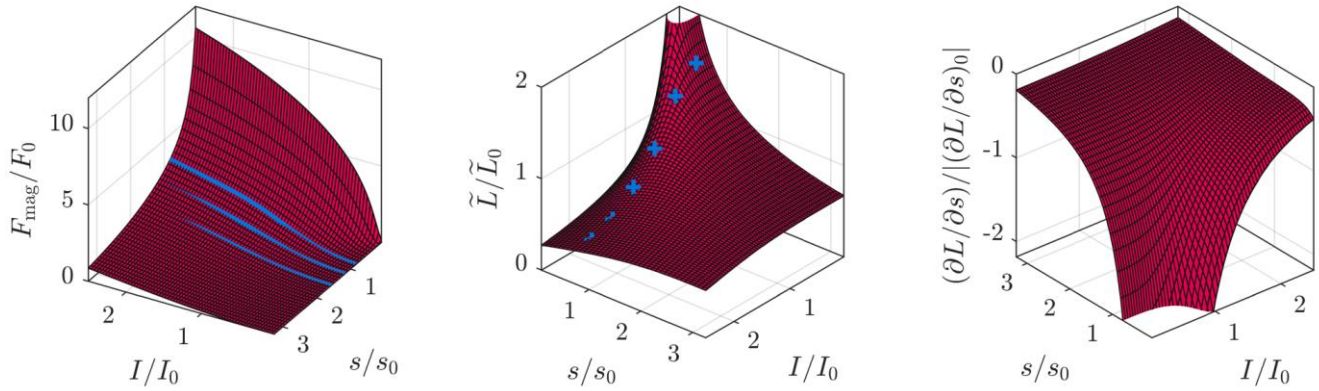

Fig. 9. Characteristic diagrams parameterizing the quantities $F_{\mathrm{mag}}(s, I_L)$, $\tilde{L}(s, I_{\mathrm{L}})$, and $\partial L(s, I_{\mathrm{L}})/\partial s$ of the simplified model for a half magnet of a standard TR09 levitation magnet. The solid blue lines and markers in the left and mid figure show the measurements from Figs. 6 and 7.

vehicle models. The models can be easily incorporated into mechatronic simulation models of the vehicle because of their well-defined input-output structure. A mechanical system model, usually a (flexible) multibody system, provides the magnets' inputs gaps and gap derivatives. The controllers provide the magnets' voltages and, in turn, use the magnets' currents and further states of the mechanical system to compute the voltage. The second output of the magnet models, i.e., the magnet forces, serves again as input for the mechanical system. This general structure of mechatronic simulation models of Maglev vehicles is shown in Fig. 10(a).

By the ongoing development process, the cross-section model of the Transrapid presented in [13, 14] is successfully equipped with guidance and levitation magnet models derived from the method introduced in Secs. II and IV. Now, the more detailed magnet models replace the former simplified models, neglecting the effects of magnetic saturation and eddy currents previously. The mechanical model describes one-eighth of a Transrapid's cross-section and maps its lateral dynamics. Its mechanics is modeled by a rigid multibody system (MBS) using Neweul-M^2 [15], an in-house developed Matlab-based MBS toolbox. The MBS includes, among others, two secondary air springs that couple the levitation chassis with the car body. The guidance and levitation magnets are attached to the levitation frame, see Fig. 10(b) for a graphical representation of the model. The overall simulation model, including the new and updated guidance and levitation magnet models, runs successfully under the reference guideway disturbances introduced in [14].

In addition, the such derived magnet models are used successfully in a novel model mapping the Transrapid's heave-pitch motion, see [16] for details. The model consists of three sections modeled by a detailed rigid MBS and moves along an infinite and periodically pillared elastic guideway, see Fig. 10(c). A so-called moving system boundary realizes the infinite guideway for which the overrunning track segments, modeled by Euler-Bernoulli beams, are used in an intelligent repetitive manner. Again, the MBS is modeled using Neweul-M^2 [15]. The model allows for studying the dynamic vehicle-guideway coupling in detail. The overall mechatronic simulation model includes individual models for the standard levitation magnets and the bow levitation magnets installed at the front and rear of the vehicle. Both magnet models are derived from the modeling technique presented in Sec. II and IV. Due to the wide validity range of the magnet models, see Figs. 6 and 7, it is possible to reliably simulate and predict various driving scenarios, e.g., magnet failures.

As pointed out in Sec. IV, the simplified current-based magnet model obtained from the numerical procedure is highly applicable for its usage in sizeable mechatronic simulation models because its computational effort is much smaller. However, the simplified magnet models assume a concentrated magnet force per underlying electric circuit and neglect the magnet's distribution along the poles mapped in detail by the flux-based model. Both magnet model types are integrated within the novel vertical model introduced in [16] to study if the usage of the simplified magnet models can be justified. The study is described in detail in [17]. Simulating the model with either the fine distribution with an individual magnet force per pole based on the detailed flux-based model or the coarse distribution with a concentrated force per underlying electric circuit reveals that the simplification is valid. The resulting vehicle dynamics coincide except for minor deviations, see [17] for details. The study outlines that it is sufficient to consider the simplified current-based magnet models within large mechatronic vehicle models. However, it is even possible to integrate the detailed flux-based model versions into comprehensive vehicle modes, which allows, e.g., to study the magnet's coupling during operation in detail, which is neglected for the simplified current-based model.

The vehicle models mentioned above use the offset-free model predictive control (MPC) concept presented in [18]. MPC is an advanced control technique which computes an optimal control input based on solving an underlying optimal control problem at each time step. The model's dynamics and even constraints can be directly considered within the optimal control problem to forecast the system behavior. The simplified current-based magnet model is well suited for such a control design due to its structure in the form of an ODE and because of its simplicity. Here, the wide validity range of the magnet

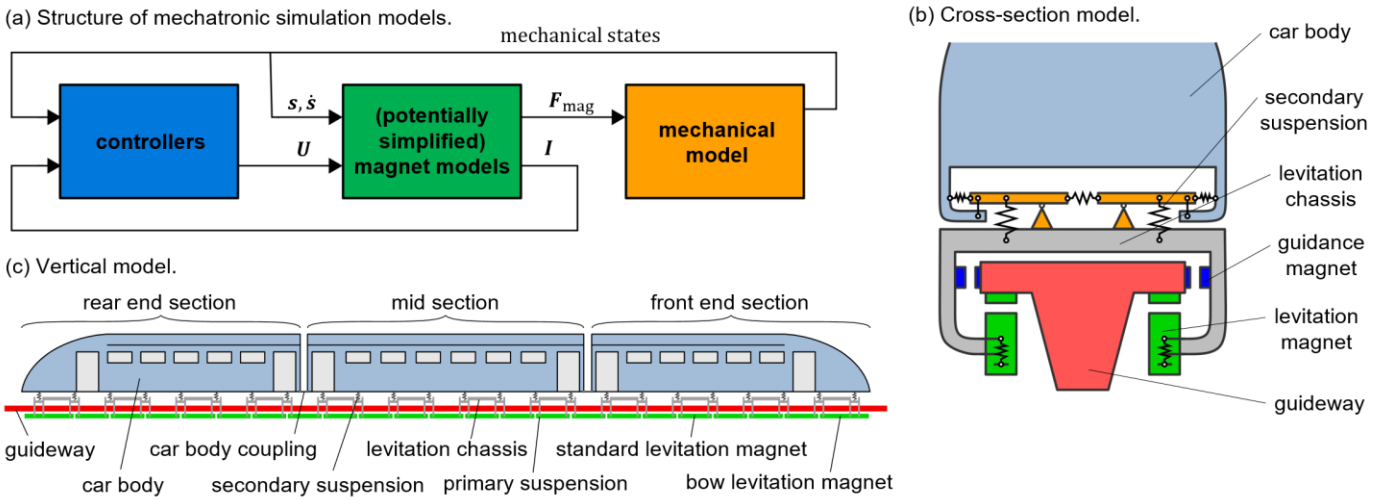

Fig. 10. General structure of mechatronic simulation models of a Transrapid Maglev vehicle (a), graphical representation of the cross-section model (b), and illustration of the vertical model (c).

models resulting from the proposed modeling technique allows for computing the magnet's control inputs reliably over the whole operating range.

VI. Conclusion

A general modeling technique for the electromagnets of EMS-based Maglev vehicles is presented. It includes effects of magnetic reluctances, fringing and leakage flux, magnetic saturation, and eddy currents. The obtained models are intended for usage in large mechatronic simulation models or for control and observer design. The models allow to study effects occurring in the magnet design process, e.g., the impact of changing dimensions, or different operating points, e.g., appearing in a failure scenario for which the extended validity range is needed. The method's strength is shown by comparison with measurements, on the one hand, exemplified by a standard levitation magnet of the latest Transrapid vehicle TR09. On the other hand, the derived magnet models are successfully incorporated into different simulation models of the vehicle and used for Maglev control design.

References

[1] H.-W. Lee, K.-C. Kim, and J. Lee, "Review of Maglev Train Technologies," *IEEE Transactions on Magnetics*, vol. 42, no. 7, pp. 1917-1925, 2006.

[2] G. Lin and X. Sheng, "Application and further Development of Maglev Transportation in China," *Transportation Systems and Technology*, vol. 4, no. 3, pp. 36-43, 2018.

[3] G. Liu and Y. Chen, "Levitation Force Analysis of Medium and Low Speed Maglev Vehicles," *Journal of Modern Transportation*, vol. 20, no. 2, pp. 93-97, 2012.

[4] J.-H. Jeong, C.-H. Ha, J. Lim, and J.-Y. Choi, "Analysis and Control of Electromagnetic Coupling Effect of Levitation and Guidance Systems for Semi-high-speed Maglev Train Considering Current Direction," *IEEE Transactions on Magnetics*, vol. 53, no. 6, pp. 1-4, 2017.

[5] H.-W. Cho, J.-S. Yu, S.-M. Jang, C.-H. Kim, J.-M. Lee, and H.-S. Han, "Equivalent Magnetic Circuit Based Levitation Force Computation of Controlled Permanent Magnet Levitation System," *IEEE Transactions on Magnetics*, vol. 48, no. 11, pp. 4038-4041, 2021.

[6] S. Ding, J. Sun, W. Han, G. Deng, F. Jiang, and C. Wang, "Modeling and Analysis of a Novel Guidance Magnet for High-Speed Maglev Train," *IEEE Access*, vol. 7, pp. 133324-133334, 2019.

[7] K. Popp and W. Schiehlen, *Ground Vehicle Dynamics*. Berlin, Germany: Springer, 2010.

[8] G. Shu and R. Meisinger, "State Estimation and Simulation of the Magnetic Levitation System of a High-Speed Maglev Train," in *Proceedings of the 2011 International Conference on Electronic and Mechanical Engineering and Information Technology (EMEIT)*, vol. 2, pp. 944-947, 2011.

[9] C.-H. Kim, J. Lim, J.-M. Lee, H.-S. Han, and D. Y. Park, "Levitation Control Design of Super-Speed Maglev Trains," in *Proceedings of the World Automation Congress (WAC)*, pp. 729-734, 2014.

[10] P. Schmid, P. Eberhard, and F. Dignath, "Nonlinear Model Predictive Control for a Maglev Vehicle regarding Magnetic Saturation and Guideway Irregularities," *IFAC-PapersOnLine*, vol. 52, no. 15, pp. 145-150, 2019.

[11] P. Schmid, G. Schneider, F. Dignath, X. Liang, and P. Eberhard, "Static and Dynamic Modeling of the Electromagnets of the Maglev Vehicle Transrapid," *IEEE Transactions on Magnetics*, vol. 57, no. 2, pp. 1-15, 2021.

[12] E. Kallenbach, R. Eick, T. Ströhla, K. Feindt, M. Kallenbach, and O. Radler, "Elektromagnete: Grundlagen, Berechnung, Entwurf und Anwendung (in German)," 5th ed. Wiesbaden, Germany: Springer-Vieweg, 2018.

[13] M. Dellnitz, F. Dignath, K. Flaßkamp, M. von Hessel, M. Krüger, R. Timmermann, and Q. Zheng, " Modelling and Analysis of the Nonlinear Dynamics of the Transrapid and Its Guideway," in *Progress in Industrial Mathematics at ECMI 2010*, vol. 17, pp. 113-123. Heidelberg, Germany: Springer, 2012.

[14] Q. Zheng, F. Dignath, P. Schmid, and P. Eberhard, "Ride Comfort Transfer Function for the Maglev Vehicle Transrapid," in *4th International Conference on Railway Technology (RAILWAYS 2018)*, 2018. Presentation slides available at http://dx.doi.org/10.18419/opus-11268.

[15] T. Kurz, P. Eberhard, C. Henninger, and W. Schiehlen, "From Neweul to Neweul-M2: Symbolical Equations of Motion for Multibody System Analysis and Synthesis," *Multibody System Dynamics*, vol. 24, no. 1, pp. 25-41, 2010.

[16] G. Schneider, P. Schmid, F. Dignath, and P. Eberhard, "Modeling and Simulation of a High-speed Maglev Vehicle on an Infinite Elastic Guideway, "in *Proceedings of the 10th ECCOMAS Thematic Conference on Multibody Dynamics*, pp. 420-431, 2022.

[17] G. Schneider, P. Schmid, F. Dignath, and P. Eberhard, "Coupled Vehicle-Guideway Dynamics Simulations of the Transrapid with Discretized Levitation Magnet Forces, " in *Proceedings of the 10th European Nonlinear Dynamics Conference (ENOC2022)*, Lyon, 2022.

[18] P. Schmid and P. Eberhard, "Offset-free Nonlinear Model Predictive Control by the Example of Maglev Vehicles, "*IFAC-PapersOnLine*, vol. 54, no. 6, pp. 83-90, 2021.